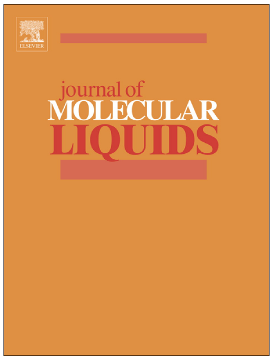

Preparation, structure and optical properties of thermochromic liquid crystal compounds containing (−)-menthyl with selective reflection

Cong-Cong Luo, Xin-Jiao Wang, Lu-Juan Han, Ying-Gang Jia, Shao-Ming Ying, Ji-Wei Wang

PII:	S0167-7322(18)35193-6
DOI:	https://doi.org/10.1016/j.molliq.2018.11.088
Reference:	MOLLIQ 9998
To appear in:	*Journal of Molecular Liquids*
Received date:	8 October 2018
Revised date:	14 November 2018
Accepted date:	19 November 2018

Please cite this article as: Cong-Cong Luo, Xin-Jiao Wang, Lu-Juan Han, Ying-Gang Jia, Shao-Ming Ying, Ji-Wei Wang , Preparation, structure and optical properties of thermochromic liquid crystal compounds containing (−)-menthyl with selective reflection. Molliq (2018), https://doi.org/10.1016/j.molliq.2018.11.088

Preparation, Structure and Optical Properties of Thermochromic Liquid Crystal Compounds containing (-)-Menthyl with Selective Reflection

Cong-Cong Luo [a], Xin-Jiao Wang [a], Lu-Juan Han [a], Ying-Gang Jia [a, *], Shao-Ming Ying [b] and Ji-Wei Wang [b, *]

[a]*College of Science, Northeastern University, Shenyang, 110004, PR China. E-mail: jiayinggang@mail.neu.edu.cn.*

[b]*Fujian Province University Key Laboratory of Green Energy and Environment Catalysis, Ningde Normal University, Ningde, Fujian, 352100, PR China, E-mail: jlwjw@sina.com*

Abstract

A series of new chiral liquid crystal compounds named **MOP*n*B** containing (-)-menthyl group has been prepared and characterized by FT-IR and ^{1}H NMR spectra. The thermal properties and optical textures were investigated by differential scanning calorimetry (DSC) and polarizing optical microscopy (POM). Increasing the length of the terminal alkoxy group tended to decrease the clearing points and narrow the temperature range of the N* phase as well as favored the development of SmC* phase. Furthermore, Bragg selective reflection spectra of the compounds were measured by ultraviolet/visible spectrometer (UV/Vis). All compounds **MOP*n*B** (*n = 2, 4, 6, 8, 10*) revealed the thermochromic property or selective reflection of visible light in the N* phase. Additionally, only **MOP10B** and **MOP12B** in the SmC* phase had the thermochromic phenomena and gave red-saffron color.

Keywords: (-)-menthol; chiral liquid crystals; selective reflection; blue phase; chiral smectic C; thermochromic

1. Introduction

Chiral liquid crystal compounds (CLCs) have been receiving growing interest as the reduced symmetry of chirality in the CLCs leads to a helical supramolecular structure, which yields some interesting properties and elegant phenomena, such as the selective reflection of light, thermochromism and ferroelectricity, rendering these periodic dielectric fluid media for a number of potential applications, particularly as thermography, tunable color filters and polarizers, reflective displays, mirrorless lasing, etc. [1-10] Due to their unique properties, many efforts have been made to fabricate novel materials with periodic structures, not only focus on the desired reflection [11], but also tuning the reflection through light [1], electricity [12, 13], stress [14], temperature [15], pH [16], solvent [17], and humidity [18]. In addition, the stimuli-responsive behavior of CLCs and their promising applications have been drawn much more attentions of scientists and engineers from different backgrounds [19-28].

In the CLC phases, there are two basic helical arrangements of the molecules. In one case, when the orientational ordering of the molecules occurs in one preferential direction, a single-twist helical structure is formed. The molecules with this structure usually show chiral nematic phase (N*) and chiral smectic C phase (SmC*). In the other case, a double-twist helical structure is created while the helix forms in more than one preferential direction, and blue phase (BP) is the typical LC phase of molecules with this structure [19]. Therefore, periodic helical structures in N*, SmC* or BP phase of CLCs induce these systems to show unique optical properties, such as Bragg selective reflection. The most striking is the so-called selective reflection, where circularly polarized light of a specific handedness and wavelength is reflected. This phenomenon can readily be observed by the naked eye as an iridescent color play when the pitch of the N* and SmC* phase structure is in the range of visible spectrum. Also in nature the selective reflection of the cholesteric-like structures is well known from the bright colors exhibited by some beetles [20]. For the cubic BPs, however, there may be several selective reflection wavelengths corresponding to various crystal planes, none of which coincide with the helical selective reflection wavelength. The selective reflection from BPs also provides iridescent light.

As the selective reflection of CLCs in visible light could generate iridescent colour, and the colour can be tuned by external stimuli, extensive studies have been conducted to design novel CLCs for practical applications. Until now, selecting or preparing novel optical active chiral entity for new CLC construction attracts many attentions of researchers. Cholesterol ($[a]_D^{20} = -36^\circ$) is one of the most widely used chiral reagents for building thermochromic CLCs. The N* and SmC* phases with the wavelength of selective reflection in the visible range of the spectrum often have a twist with a pitch P well below $P < 1$ μm [21]. And also, to generate BPs, molecules require high chirality [22-24]. BPs are generally observed between the isotropic phase and the cholesteric or smectic phases of highly chiral mesogens, where the N* phase at lower temperature often exhibits selective reflection in the visible range. That is, short pitch is essential for them.

Optically active (-)-menthol has three chiral centers and shows a large specific rotation of -50˚ ($[a]_D^{20}$ = -50˚), which can cause the plane of polarization to rotate greatly, so we expect that CLCs containing (-)-menthyl possess a short pitch in mesophase for generating BPs and N*/SmC* with thermochromic properties. Recently, we have successfully synthesized CLCs based on (-)-menthol by introducing oxyacetyloxy spacer (-OCH_2COO-) [25-29] or succinyloxy group (-$OOCCH_2CH_2COO$-) [30-32] between the mesogenic core and the bulky terminal menthyl group. And these CLCs reveal BPs and thermochromic properties in N* phase. In this study, we synthesised a series of new CLCs **MOP*n*B** (*n = 2 – 18*) with various terminal chain lengths and investigated the effect of chain lengths on the thermal properties and pitches of CLCs. In this series, the alkoxy terminal group is substituted with *n*-ethoxy, *n*-butyloxy to *n*-octadecaneloxy tails in even numbers (*n*). We found that different lengths of terminal alkoxy groups have a significant influence on the selective reflection and thermal properties. Furthermore, we also discussed the influence of the structure of alkoxy terminal groups on the mesomorphism and thermochromism of the CLCs in detail.

2. Experimental

2.1 Materials

(-)-Menthol was purchased from Shanghai Kabo Chemical Co., Ltd. Succinic anhydride, 1-bromobutane, 1-bromohexane, 1-bromooctane, 1-bromodecane, 1-bromododecane, 1-bromotetradecane, 1-bramohexadecane, 1-bromooctadecane, 4-hydroxybenzoic acid, ethyl 4-hydroxybenzoate, 4-ethoxylbenzoic acid and other reagents and solvents were all purchased from Sinopharm Chemical Reagent Co., Ltd. All reagents were used directly without further purification. Solvents were purified by standard methods.

2.2 Characterization

The chemical structure of intermediates and CLCs were analyzed by proton magnetic resonance spectroscopy using a Bruker ARX400 spectrometer with deuterated chloroform as a solvent and tetramethylene silane (TMS) as internal standard. Fourier transform infrared (FT-IR) spectra of the synthesized intermediates and CLCs in solid state were obtained by the KBr method performed on PerkinElmer spectrum One spectrometer (PerkinElmer, Foster City, CA). Transition temperatures and enthalpies were measured by a DSC 204 (Netzsch, Hanau, Germany) equipped with a cooling system. The optical textures of mesophases were identified by polarizing optical microscopy (Leica, Germany) with a Linkam cooling and heating stage. XRD measurements were performed with a nickel-filtered Cu-*Ka* radiation (Rigaku, Japan). The selective reflection wavelength was measured using a PerkinElmer 950 ultraviolet/visible (UV/Vis) spectrometer with hot stage.

2.3 Synthesis of the intermediates and CLCs

The synthetic procedures of all the intermediates and CLCs are shown in scheme 1. Intermediate compound, 4-hydroxyphenyl 4-(4-menthyloxy-4-oxobutanoyloxy) benzoate (**3**) was prepared according to our previous reports [31]. Intermediates 4-alkoxybenzoic acids **5-***n* (*n = 4, 6, 8, 10, 12, 14, 16, 18*) were synthesised via previously published methods (**5-**2 was purchased from Sinopharm Chemical Reagent Co. ,Ltd. directly) [33].

All the CLCs 4-(4-(4-menthyloxy-4-oxobutanoyloxy)benzoyloxy)phenyl 4-alkoxylbenzoate (**MOP*n*B**) were synthesised by the Steglich esterification reaction. 4-Alkoxy benzoic acids with intermediate **3** were catalyzed by N,N´-dicyclohexyl carbodiimide (DCC) and N,N´-dimethylaminopyridine (DMAP) to prepare CLCs **MOP*n*B** (*n = 2 – 18*) series. The detailed synthetic procedures and characterizations of CLCs were described in the Supporting Information.

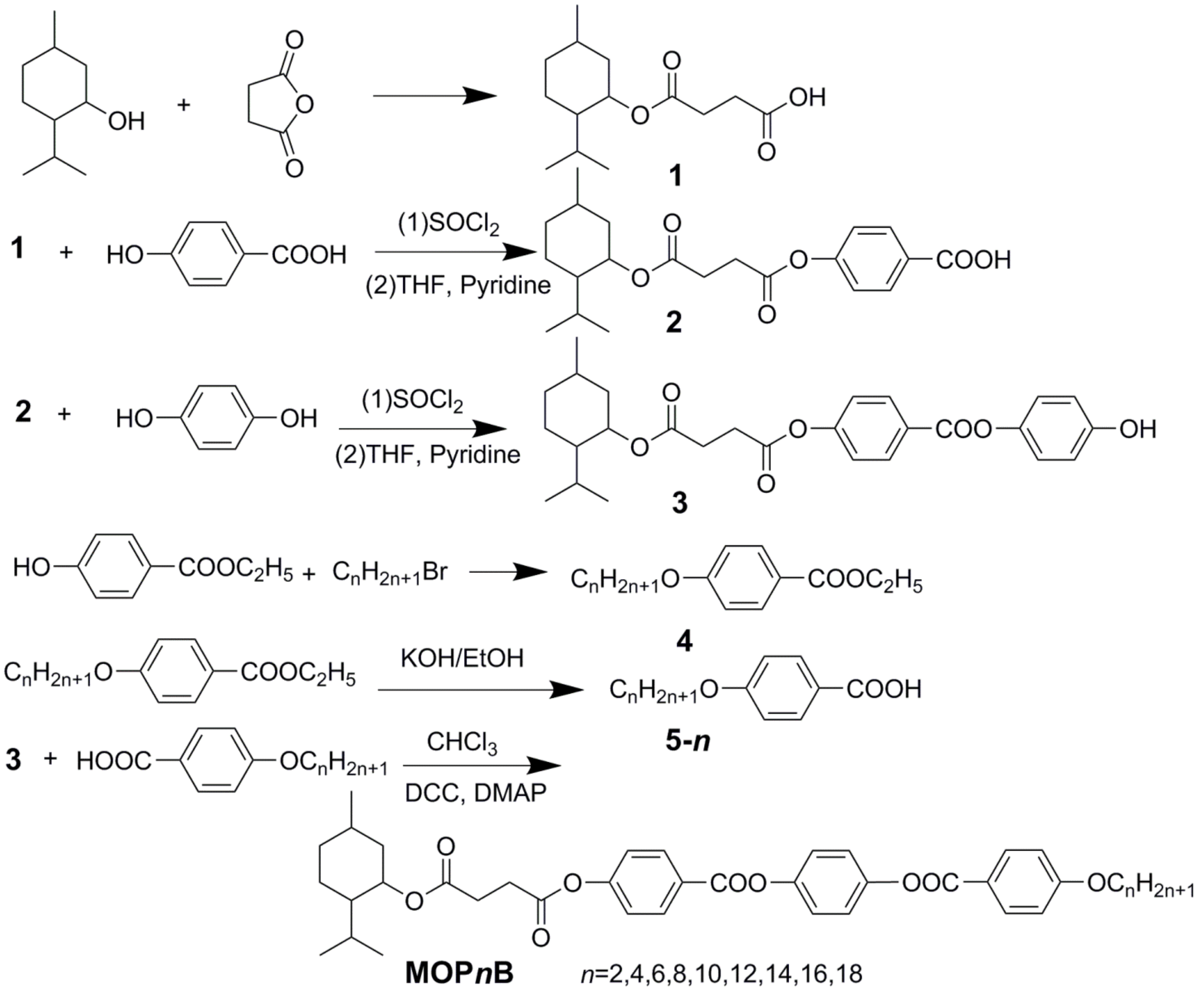

Scheme 1. Synthesis of the compounds **MOP*n*B** (*n=2, 4, 6, 8, 10, 12, 14, 16, 18*)

3. Results and discussion

3.1 Elucidation of molecular structures

The series of CLCs based on menthol were designed as target compounds, in which the terminal alkoxy groups increased in even carbon numbers from 2 to 18. The structures of new CLCs **MOP*n*B** (*n = 2 – 18*) were characterised by FT-IR and ^{1}H NMR. FT-IR measurements confirmed the formation of the compounds. In the IR spectra, we can see that the hydroxyl stretching absorption band of intermediate **3** disappear; meanwhile, ester stretching bands move to around 1731, 1764 cm^{-1} for all CLCs (Fig. 1). The representative ^{1}H NMR spectrum of compound **MOP10B** is given in Fig. 2. In the ^{1}H NMR spectra, all signals of protons were assigned well for the proposed structures. Especially, the proton of aryl skeleton exhibits three multiplets and one symmetrical doublet, indicating the mesogenic core section of **MOP10B**. Additionally, the signal δ 4.78 – 4.72 ppm corresponds to the proton of menthyl group linking to ester group, and δ 4.07 – 4.00 ppm corresponds to methylene protons in alkoxy section. And 2.94 – 2.91, 2.78 – 2.74 ppm corresponds to four protons of methylene in the succinyloxy group. All the characteristic data are in accordance with the proposed structures of the compound **MOP10B**.

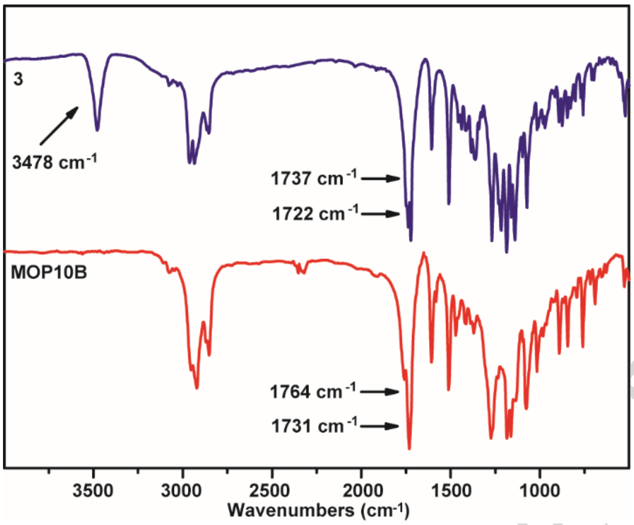

Figure 1. IR spectra of intermediate **3** and compound **MOP10B**.

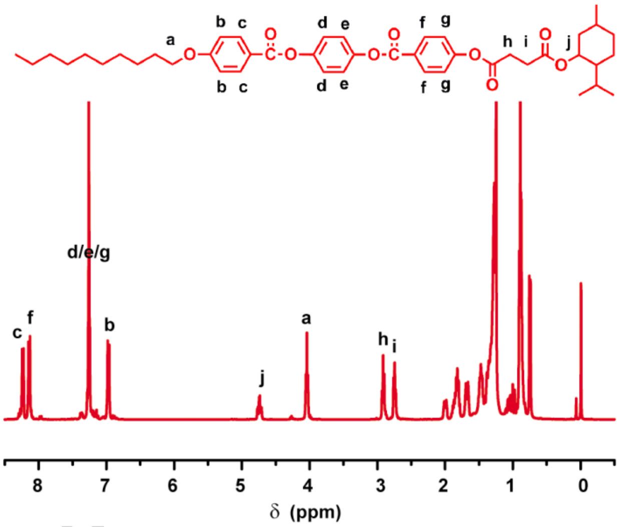

Figure 2. The ^{1}H NMR spectrum of compound **MOP10B**.

3.2 Thermal analysis

The thermal properties of the new CLCs with different alkoxy tails were detected by DSC. The phase transition temperatures were measured at a rate of 10 °C min^{-1} on the first heating and cooling cycles and Figure 3 shows the DSC curves for **MOP2B** and **MOP10B** as examples. Their phase sequences, transition temperatures and enthalpies of the **MOP*n*B** (*n = 2 – 18*) are presented in Table 1.

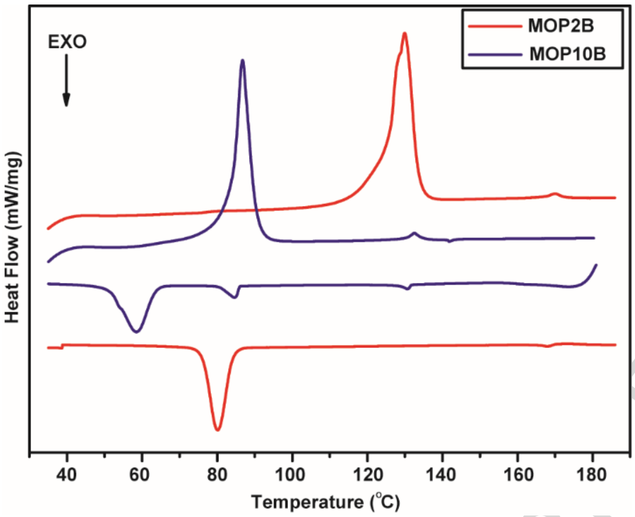

Figure 3. DSC thermograms of compounds **MOP2B** and **MOP10B**.

Table 1. Transition Temperatures (°C) and Enthalpies (J/g) of **MOP*n*B** series

n	Phase transitions[a] °C (corresponding enthalpy changes[b]; J g^{-1})	
	heating	cooling
2	Cr129.9(71.27)N*170.2(0.62)Iso	Iso168.1(0.59)BP164.5[c]N*80.1(48.66)Cr
4	Cr111.6(52.66)N*148.3(0.75)Iso	Iso147.0(0.81)BP144.7[c]N*68.7(22.37)Cr
6	Cr107.0(53.80)N*142.7(0.81)Iso	Iso139.4(0.87)BP138.8[c]N*66.3(47.57)Cr
8	Cr120.7(46.84)N*138.0(1.21)Iso	Iso135.0(1.00)BP134.2[c]N*76.0(46.02)Cr
10	Cr86.8(51.23)N*132.6(1.29)Iso	Iso130.7(1.24)BP129.6[c]N*84.6(4.31)TGBA*83.6[c]SmA*83.4[c]SmC*58.4(38.22)Cr
12	Cr105.5(72.8)N*124.3(0.89)Iso	Iso122.2(0.92)BP121.9[c]N*86.0(3.45)TGBA*85.8[c]SmA*77.2[c]SmC*61.1(22.67)Cr
14	Cr109.0(71.78)N*120.6(0.65)Iso	Iso118.4(0.96)BP117.5[c]N*90.7(3.48)SmC*70.0(36.74)Cr
16	Cr96.8(47.74)N*110.7(0.37)Iso	Iso108.0(0.33)BP107.4[c]N*84.9(0.58)SmC*69.5(39.61)Cr
18	Cr104.6(57.08)N*111.0(0.10)Iso	Iso110.0(0.99)BP109.7[c]N*94.0(3.30)SmC*78.7(58.82)Cr

[a]Phase transition temperatures determined by both POM and peak values of the DSC traces. [b]Values of enthalpy are given in brackets. *n* indicates the number of carbon atoms in the terminal alkoxy chains. [c]The transition seen under POM was too weak to be recognized by DSC.

For **MOP*n*B** (*n = 2, 4, 6, 8*), DSC heating thermograms show not only a melting transition, but also a chiral nematic phase (N*) to isotropic phase (Iso) transition on heating cycles. On the cooling cycles, an isotropic to N* phase transition and a crystallization phase transition (Cr) were observed. **MOP*n*B** (*n = 10, 12, 14, 16, 18*) have the same phase transition to **MOP*n*B** (*n = 2, 4, 6, 8*) on heating and cooling cycles, but as an unusual, the monotropic chiral smectic C phase (SmC*) phase after N* phase in compounds **MOP*n*B** (*n = 10, 12, 14, 16, 18*) appear while cooling the samples from their isotropic phase. In addition, the enthalpies of all compounds **MOP*n*B** in Table 1 gave lower values irrespective of the length of the alkoxy chains. This may be accounted in terms of the reduction of length-to-breadth ratio and the increased biaxiality arising from the orientation of the menthyl group with respect to the long axes of the mesogenic unit, which could reduce the transition temperatures and enthalpies [34-37].

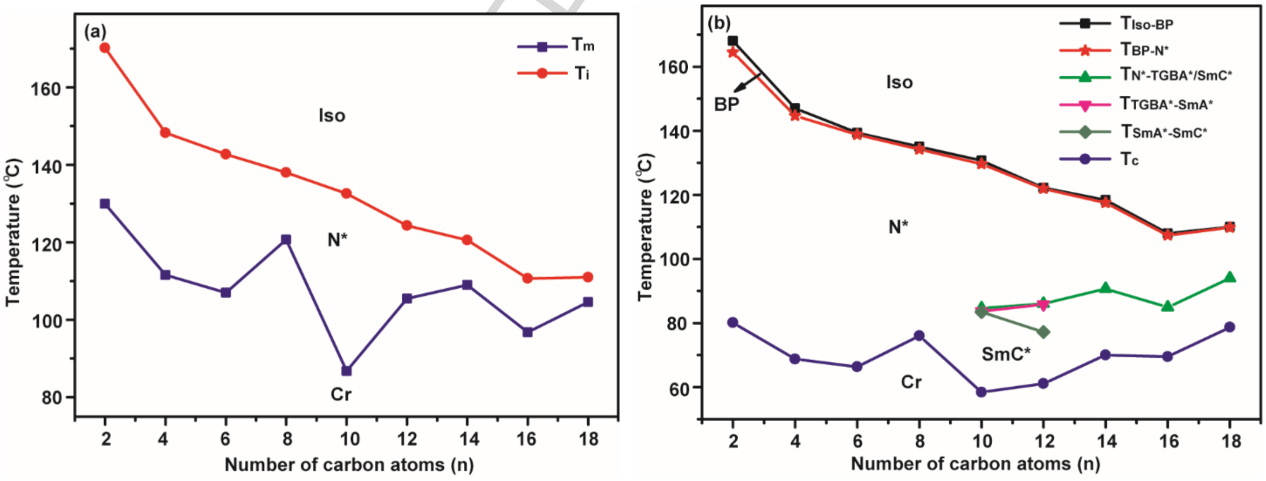

Figure 4. A plot of transition temperature as a function of number of carbon atoms (*n*) in the terminal alkoxy groups for **MOP*n*B** series: (a) heating mode and (b) cooling mode.

The relationship of phase transition temperatures (heating and cooling mode) with different lengths of the terminal alkoxys (*n*) is presented in Figure 4. The number *n* in alkoxys has a modest influence on the mesomorphic properties. It shows that increasing the lengths in alkoxy groups changs the transition temperature and the mesomorphic temperature ranges. The clearing points (T_i) and the phase transition temperature of Iso – N* transition decrease with increasing *n*. The effect of increasing the length of terminal alkoxys is two-fold; first, the anisotropic properties of the molecule are increased resulting in an increased temperature of T_i and Iso – N* transition; second, the dilution of the cores is increased resulting in a decrease in T_i and Iso – N* transition. Thus, the overall effect of increasing the length of a terminal alkoxys depends essentially on the interaction strength parameter of the core [37, 38]. In our case, the core of a three ring system of **MOP*n*B** (*n = 2 – 18*) is large, thus the dilution effect dominates and the transition temperatures simply fall more or less with increasing chain length. Figure 4 also revealed that **MOP2B** – **MOP8B** are enantiotropic N* liquid crystal compounds. But **MOP10B** – **MOP18B** show not only enantiotropic N* phase but also monotropic SmC* phase. And the N* – SmC* transition temperatures are found to rise gently. The temperature range of the N* phase narrows, whereas the thermal stability of the SmC* phase gradually increases with *n* increasing. This identifies that the increase of alkoxy groups favours the formation of SmC* phase over N* phase, presumably due to the enhanced interlayer interactions derived from the increase of the terminal alkoxy groups [39].

3.3 Optical analysis

The optical textures for studied compounds **MOP*n*B** (*n = 2 – 18*) were characterized by POM for identifying their mesophase. Their thermochromic property or selective reflection in visible light was analysed by UV-vis spectrometer. In **MOP*n*B** (*n = 2 – 18*) series, all compounds show a phase transition sequence of Cr – N* – Iso on heating cycles. During slowly cooling, compounds **MOP*n*B** (*n = 2, 4, 6, 8*) show Iso – BP – N* – Cr; **MOP10B** and **MOP12B** exhibit two new phase transitions of twist grain boundary A (TGBA*) and chiral smectic A phase (SmA*) and present a phase transition sequence of Iso – BP – N* – TGBA* – SmA* – SmC* – Cr; and **MOP*n*B** (*n = 14, 16, 18*) reveal a phase transition sequence of Iso – BP – N* – SmC* – Cr. The differences of measurement results between DSC and POM were the BP, TGBA* and SmA* phases which were only observed by POM. Because the Iso – BP and N* – TGBA* – SmA* transitions are too weak to record in the DSC measurements.

3.3.1 CLCs MOP2B, MOP4B, MOP6B and MOP8B

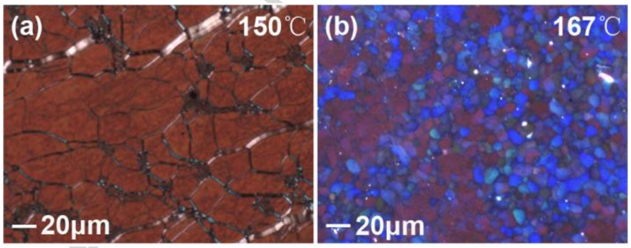

Figure 5. Optical textures of **MOP2B**

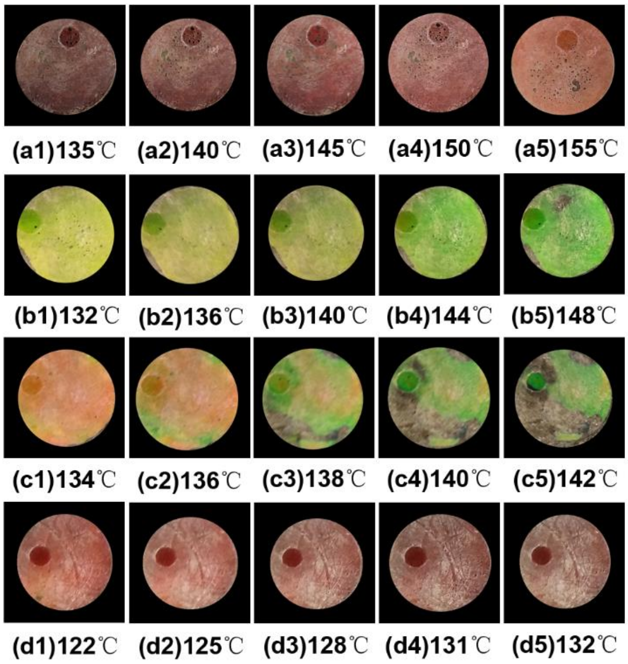

Figure 6. Sets of photographs of thermochromic process produced by **MOP2B** (a), **MOP4B** (b), **MOP6B** (c) and **MOP8B** (d) on heating process in the N* phase.

Compounds **MOP*n*B** (*n* = *2, 4, 6, 8*), while slowly heating from their melting points, display the planar oily streak texture (Fig. 5a). The planar texture of the N* phase exhibits an important optical phenomena, the selective reflection. In general, the selective reflection wavelength depends on the molecular chirality and ordering of the molecules within the phase. Due to the unique helical structure of N* phase, their orientation of the molecules varies in a helical fashion and thus selectively reflects light according to Bragg's law [40]. The variation of temperature resulted in the change of *P*, and led to the thermochromic character (selective reflection) at different temperatures and different observation angles. This is the reason for CLCs having thermochromic phenomena, which can readily be observed by the naked eye as an iridescent colour. As a representative, sets of photographs of thermochromic process for compounds **MOP*n*B** (*n* = *2* – *8*) on heating process in the N* phase are shown in Figure 6. The color of the reflected light of compounds **MOP2B** and **MOP8B** are varied in the red region. Then compounds **MOP4B** and **MOP6B** are in the yellow-green or red-green region.

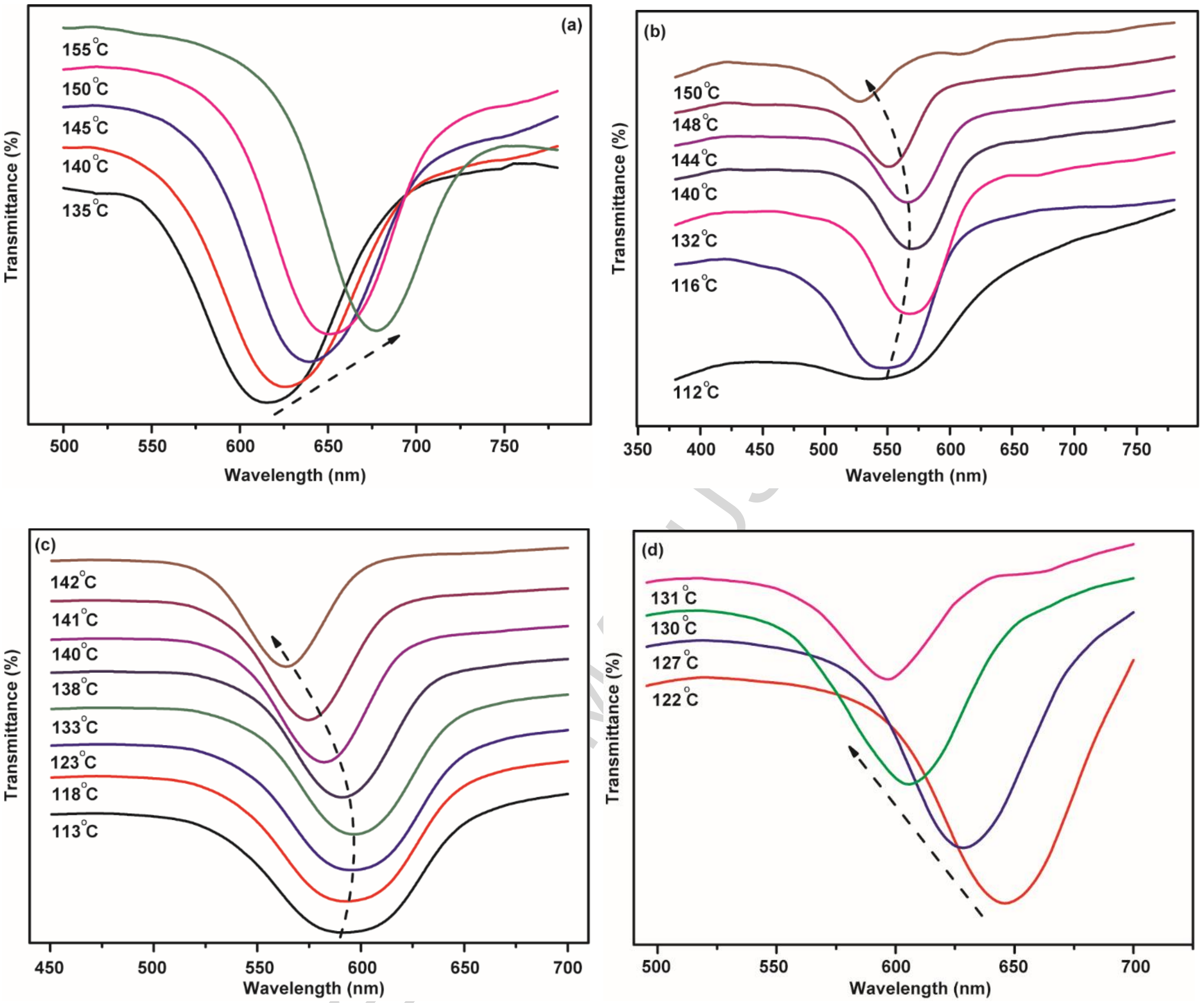

Figure 7. UV/Vis spectra of **MOP2B** (a), **MOP4B** (b), **MOP6B** (c) and **MOP8B** (d).

Selective reflection requires the light with the same handedness as the helix and the wavelength satisfying $\lambda = nP$, where n is an average refractive index, λ is the maximum wavelength. The representative reflection spectra of **MOP2B** in the N* phase on heating cycles are shown in Figure 7a. Based on the observations, we can estimate the selective reflection wavelength changing from 617 nm to 677 nm upon increasing temperature with the temperature interval from 135 °C to 160 °C for **MOP2B**. With the temperature increasing, the reflective colours of the N* phase show an obvious red shift, which is caused by the Bragg selective reflection from the plane of oily streak textures of the N* phase. This red shift phenomenon of N* phase with the increase of temperature has been reported before [41]. The reflection colours of **MOP2B** mainly shift to a long-wavelength region with the increasing of temperature due to the *P* of N* phase altered with temperature and it unwound with increasing temperature. However, the selective reflection wavelengths of **MOP4B** and **MOP6B** revealed a slight red-shift firstly with increasing temperature, until closing to the clearing point, the wavelengths show blue shift (Fig. 7b-7c). Further, the obvious blue shift was observed by compound **MOP8B**. The wavelengths of **MOP8B** shift 49 nm with increasing temperature (Fig. 7d). The reason for blue shift with increasing temperature was that the helical structure started to twist. So, the wavelengths may have red shift or blue shift with increasing the temperature in the N* phase of CLCs **MOP*n*B** (*n = 2 – 8*).

On the cooling cycles for **MOP*n*B** (*n = 2 – 8*), the BP appeared firstly as an iridescent platelet texture with a small temperature range about ~4 °C between isotropic and N* phases as shown in Figure 4b. Their allure and beauty mesophases originate mainly from their self-organized three-dimensional photonic crystal structure. With the lattice spacing on the order of several hundred nanometers, Bragg selective reflection could be any colour positioned in the visible region [43]. The high chirality of (-)-menthyl in CLCs forces the mesogenic molecules to twist with respect to each other, resulting in the typical double twisted cylinder of BPs. Defect theory well explains why BPs are usually found to appear in a narrow temperature range (Seen in the SI). On further cooling, the focal conic texture of N* phase with a wider temperature range could be observed until the sample crystallized.

3.3.2 CLCs MOP10B and MOP12B

Compounds **MOP*n*B** (*n = 10, 12*) also display the oily streak textures on the heating cycles (Fig. 8a). Based on the observation, the texture contains coloured grains, with the colour corresponding to the pitch length of the N* helix. The N* phase of **MOP10B** exhibits reflections in the red region. The representative thermochromic image of **MOP10B** is shown in Figure 8b. The mesomorphic properties and the thermochromic phenomena disappear at 132.6 °C (Fig. 8c) and UV-Vis spectra of N* phase for **MOP10B** is shown in Figure 8d. We can estimate the value of the wavelength changing from 752 nm to 652 nm upon increasing temperature within the temperature interval from 114 °C to 130 °C. The helical structure started to wind with increasing temperature. The plot of wavelength against temperature showed a linear relationship, and $d\lambda/dT < 0$ in the N* phase for **MOP10B**. As the length of the alkoxy increases, the helical pitch length of the N* phase increases gradually, and when *n* = 12, the pitch length of the N* phase of this series CLCs is out of the order of the wavelength of white light, so no selective reflection in N* phase of **MOP12B** appears.

When slowly cooling from isotropic phase for **MOP10B** and **MOP12B**, the BP appears as a fuzzy blue texture with a small temperature range about 0.5 °C between isotropic and N* phases. Since the range of BP phase is too narrow, the fully structure of BP phase cannot formed. On further cooling, the focal conic texture of N* phase also grew (Fig. 9a). As the temperature continued to cool down from the N* phase, the filament texture appeared (Fig. 9b), indicating the characteristic of TGBA* phase. And then the SmA* phase was confirmed by the microscopic observation of a dark field of view for homeotropic orientation (Fig. 9c). Similar to the short pitch cholesteric phase, the short pitch SmC* phase exhibits the phenomenon of selective reflection as well. On further cooling, the SmC* phase appeared with selective reflection as the temperature declined and the equivalent POM, thermochromic images and UV-Vis spectra in SmC* phase for **MOP10B** are shown in Figure 9d-9f. First, the red petal texture (Fig. 9d (1)) started growing and with further cooling other colour petal textures (Fig. 9e (1) - f (1)) formed. For SmC* phase, where the pitch length of the helix is of a similar magnitude to the wavelength of light, light will be selectively reflected. Through the reflected image we found that the thermochromic process in cooling stage passes through red (Fig. 9d (2)) to saffron (Fig. 9f (2)) for **MOP10B**. The corresponding value of reflection wavelength changes from 703 nm (Fig. 9d (3)) to 581 nm (Fig. 9f (3)) with the temperature interval from 80 °C to 70 °C. The reflection wavelengths of **MOP10B** in SmC* phase are mainly blue shift with decreasing the temperature. The colours of petal textures, reflected colour and reflection wavelength changed with temperature caused by the variation of helical pitches with changing temperature in the visible region of the spectra [44]. The reason for this outcome is that the molecules are tilted at an angle with respect to the layer planes, and the tilt angle (θ) in SmC* phase usually increases as the temperature decreases. Generally, after the SmA* – SmC* phase transition, the tilt θ varies with respect to temperature in the following:

$$\theta(T) = \theta_0(T_N - T)^{0.5}$$

Where T_N is the phase transition temperature, T is the temperature, θ_0 is a constant. Thus, the tilt angle θ increases as the temperature is reduced, and as a consequence the pitch in a helical SmC* is shortened. CLC **MOP12B** also displays similar texture and thermochromic phenomena in SmC* phase with **MOP10B**, however, the temperature ranges of iridescent colours for **MOP12B** are a little narrower than that of **MOP10B**. On further cooling, the CLCs **MOP10B** and **MOP12B** began to crystallize.

Both N* phase and SmC* phase with short pitch exhibit the phenomenon of selective reflection. **MOP10B** in both N* and SmC* phases can reveal thermochromic phenomena through its spectral range, but **MOP12B** is only observed thermochromic process in SmC* phase.

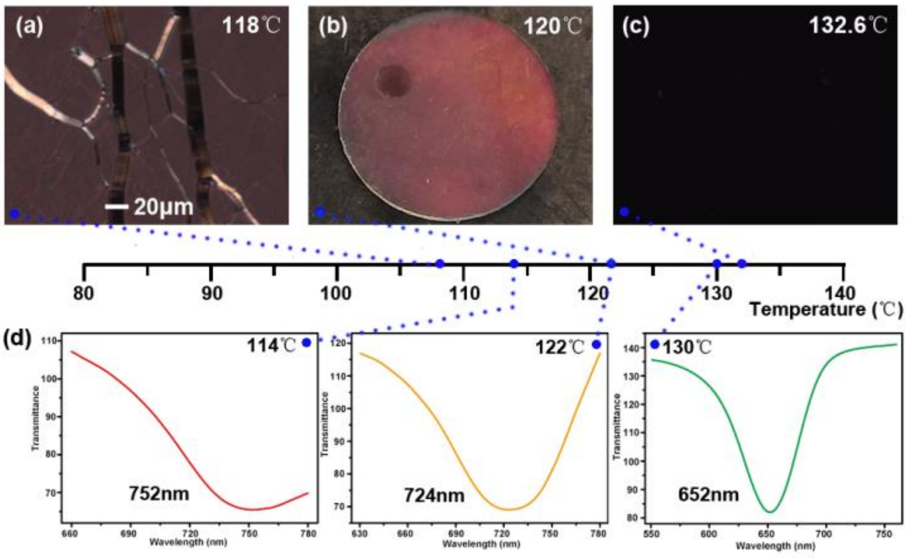

Figure 8. Optical textures and reflection spectra of **MOP10B** in N* phase on heating.

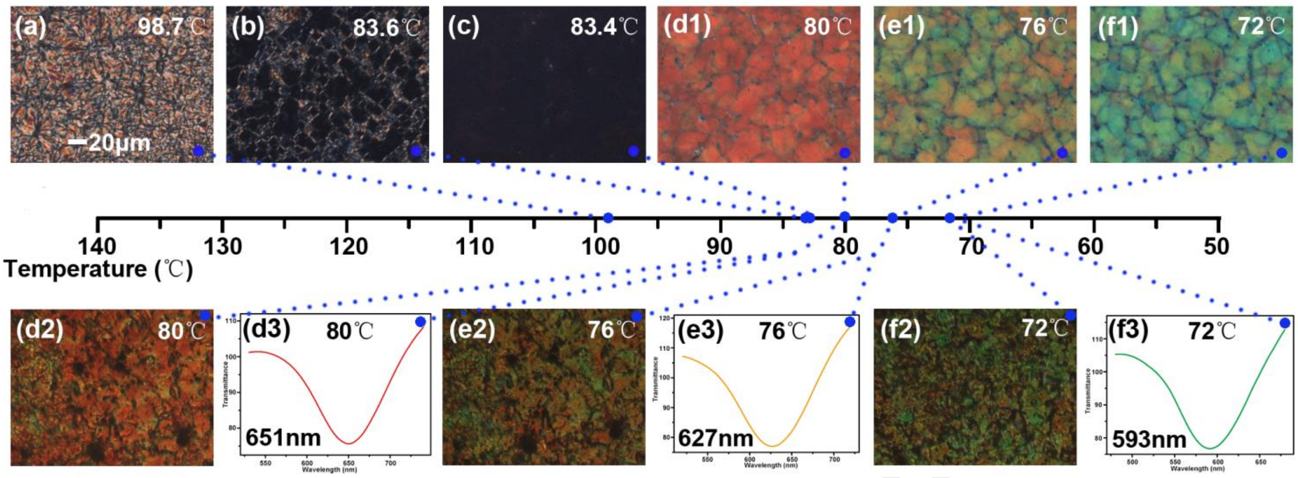

Figure 9. Optical textures of **MOP10B** in N* phase (a), TGBA* phase (b) and SmA* phase (c). And the equivalent POM, reflected images and UV/vis spectra in SmC* phase on cooling to 80 °C (d), 76 °C (e) and 72 °C (f).

3.3.3 CLCs MOP14B，MOP16B and MOP18B

Compounds **MOP*n*B** (*n = 14, 16, 18*) also displayed oily streak texture on heating cycles. On slowly cooling from their isotropic phases, the BP appeared as a fuzzy blue texture with increasing alkoxy chain length. This suggested that extending the terminal alkoxy chain length could increase the intermolecular interaction such that it limited the formation of the BP in this series. Typically, the compounds were found to exhibit N* phase which possessed focal conic textures on cooling cycles. Subsequently cooling of the N* phase produced a transition to the SmC* phase which exhibited fingerprint texture for **MOP14B** and **MOP16B** (Fig. 10a) and bonnet texture for **MOP18B** (Fig. 10b).

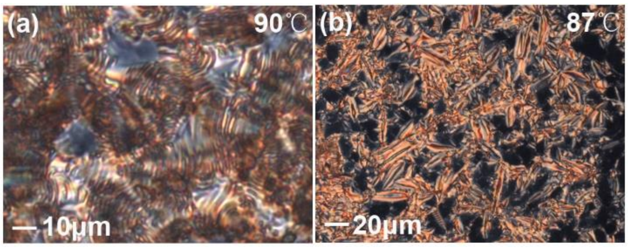

Figure 10. Optical textures of **MOP14B** and **MOP18B**.

The short pitch N* phase or SmC* phase exhibits the phenomenon of selective reflection, and N* phases with a pitch smaller than approximately $P < 1$ μm are generally referred to as short pitch materials. As the length of the alkoxy increases, the helical pitch increases gradually and long pitch N* phase or SmC* phase forms. Due to the pitch length of these phases is out of the order of the wavelength of white light, so no selective reflection of **MOP14B**, **MOP16B** and **MOP18B** appears.

3.4 XRD studies

To ascertain the mesophase assignments of the N* and SmC* phases, XRD measurements were carried out for the sample **MOP10B**. The sample was filled into a Lindemann capillary (1 mm diameter) tube in the isotropic phase and both ends of the tube were flame sealed. The diffraction patterns in the mesophase obtained on cooling from their isotropic phases were collected on an image plates. The intensity versus 2θ plots derived from the diffraction patterns of **MOP10B** are shown in Figure 11. At 110 °C, a broad diffraction peak was observed in the large-angle region ($2\theta = 19.3°$), corresponding to the intermolecular distance of 4.59 Å, which is assigned to the N* phase. When it cooled from 110 °C to 82 °C, the diffraction pattern showed a sharp diffraction peak $2\theta = 2.6°$ (d-spacing 33.9 Å) and a diffused peak at $2\theta = 19.2°$ (d-spacing 4.62 Å). The sharp diffraction peak in the small-angle region is characteristic of smectic structures, while the diffused peak indicates the lateral packing. The length of the molecule (*l*) including alkoxy groups in all *trans* conformation of **MOP10B** measured using a Chem3D molecular model was estimated to be 38 Å. The tested *d*-spacing at 82 °C is less than the molecular length, suggesting a titled smectic C molecular arrangement. When it cooled from 82 °C to 75 °C, the interlayer distance decreased from 33.9 Å to 32.68 Å. The tilt angle (α) is calculated to be 29.8° at 82 °C and 34.1° at 75 °C from the equation $\alpha = \cos^{-1}(d/l)$. The *d*-spacing at 70 °C does not change, but the intensity of the peak was significantly enhanced, which demonstrated that the order of molecule arrangement enhanced in intermolecular layers at 70 °C [45].

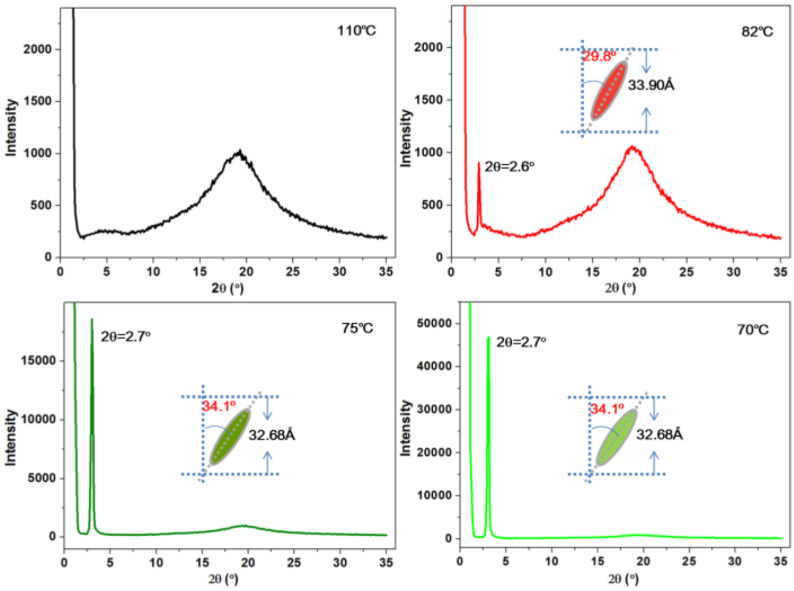

Figure 11. Intensity versus 2θ graph derived from the XRD diffraction of compound **MOP10B** at 110 °C, 82 °C, 75 °C and 70 °C, respectively.

4. Conclusions

In this work, we have synthesized a series of new CLC compounds **MOP*n*B** (*n = 2 – 18*) derived from (-)-menthol and investigated their mesomorphism and optical properties. In general, the compounds **MOP*n*B** (*n = 2 – 18*) all exhibit oily streak textures on heating cycles. Upon cooling, the compounds **MOP*n*B** (*n = 2 – 8*) exhibit a phase transition sequence as Iso – BP – N* – Cr; compounds **MOP*n*B** (*n = 10, 12*) reveal an Iso – BP – N* – TGBA* – SmA* – SmC* – Cr phase transition process; **MOP*n*B** (*n = 14, 16, 18*) reveal a phase transition sequence of Iso – BP – N* – SmC* – Cr. And with increasing the length of the terminal alkoxy tail, the corresponding T_i and the phase transition temperature of Iso – N* decrease. The temperature range of the N* phase narrows and the thermal stability of the SmC* phase gradually increases with the increase of *n*. CLCs **MOP*n*B** (*n = 2 – 10*) in N* phase reveal thermochromic phenomena due to the selective reflection of visible light, however, when n ≥ 12, thermochromic phenomena in N* phase disappear. Additionally, iridescent petal textures with thermochromic process in SmC* phase were only observed for **MOP10B** and **MOP12B**, and the wavelengths are blue shift with decreasing temperature. CLC **MOP10B** reflects selectively visible light or reveals thermochromic property not only in N* phase but also in SmC* phase. High chirality and high twist power are approved for (-)-menthol and it is a good candidate for preparation of CLCs with BPs or short pitch.

Acknowledgements

This work was supported by National Nature Science Foundation of China (31560268) and Program for New Century Excellent Talents in Fujian Province University (JA14325).

References

[1] H. K. Bisoyi, Q. Li. Light-Directing Chiral Liquid Crystal Nanostructures: From 1D to 3D, Accounts of Chemical Research. 47 (2014) 3184-3195.

[2] H. K. Bisoyi, Q. Li. Light-Directed Dynamic Chirality Inversion in Functional Self-Organized Helical Superstructures, Angewandte Chemie-International Edition. 55 (2016) 2994-3010.

[3] H. Coles, S. Morris. Liquid-crystal lasers, Nature Photonics. 4 (2010) 676-685.

[4] Y. N. Li, C. M. Xue, M. F. Wang, et al. Photodynamic Chiral Molecular Switches with Thermal Stability: From Reflection Wavelength Tuning to Handedness Inversion of Self-Organized Helical Superstructures, Angewandte Chemie-International Edition. 52 (2013) 13703-13707.

[5] S. Pieraccini, S. Masiero, A. Ferrarini, et al. Chirality transfer across length-scales in nematic liquid crystals: fundamentals and applications, Chemical Society Reviews. 40 (2011) 258-271.

[6] L. Wang, Q. Li. Stimuli-Directing Self-Organized 3D Liquid-Crystalline Nanostructures: From Materials Design to Photonic Applications, Advanced Functional Materials. 26 (2016) 10-28.

[7] Y. Wang, Q. Li. Light-Driven Chiral Molecular Switches or Motors in Liquid Crystals, Advanced Materials. 24 (2012) 1926-1945.

[8] Z. G. Zheng, Y. N. Li, H. K. Bisoyi, et al. Three-dimensional control of the helical axis of a chiral nematic liquid crystal by light, Nature. 531 (2016) 352-357.

[9] F. Ahmad, M. Jamil, Y. J. Jeon. Reverse mode polymer stabilized cholesteric texture (PSCT) light shutter display - A short review, Journal of Molecular Liquids. 233 (2017) 187-196.

[10] S. Kobayashi, Y. Shiraishi, N. Toshima, et al. Further study of optical homogeneous effects in nanoparticle embedded liquid-crystal devices, Journal of Molecular Liquids. 267 (2018) 303-307.

[11] K. E. Shopsowitz, H. Qi, W. Y. Hamad, et al. Free-standing mesoporous silica films with tunable chiral nematic structures, Nature. 468 (2010) 422-U246.

[12] S. Tokunaga, Y. Itoh, Y. Yaguchi, et al. Electrophoretic Deposition for Cholesteric Liquid-Crystalline Devices with Memory and Modulation of Reflection Colors, Advanced Materials. 28 (2016) 4077-4083.

[13] J. Xiang, Y. N. Li, Q. Li, et al. Electrically Tunable Selective Reflection of Light from Ultraviolet to Visible and Infrared by Heliconical Cholesterics, Advanced Materials. 27 (2015) 3014-3018.

[14] D. T. Ge, E. Lee, L. L. Yang, et al. A Robust Smart Window: Reversibly Switching from High Transparency to Angle-Independent Structural Color Display, Advanced Materials. 27 (2015) 2489-2495.

[15] Y. Ohtsuka, T. Seki, Y. Takeoka. Thermally Tunable Hydrogels Displaying Angle-Independent Structural Colors, Angewandte Chemie-International Edition. 54 (2015) 15368-15373.

[16] J. E. Stumpel, E. R. Gil, A. B. Spoelstra, et al. Stimuli-Responsive Materials Based on Interpenetrating Polymer Liquid Crystal Hydrogels, Advanced Functional Materials. 25 (2015) 3314-3320.

[17] M. K. Khan, A. Bsoul, K. Walus, et al. Photonic Patterns Printed in Chiral Nematic Mesoporous Resins, Angewandte Chemie-International Edition. 54 (2015) 4304-4308.

[18] K. Szendrei, P. Ganter, O. Sànchez-Sobrado, et al. Touchless Optical Finger Motion Tracking Based on 2D Nanosheets with Giant Moisture Responsiveness, Advanced Materials. 27 (2015) 6341-6348.

[19] L. Wang, Q. Li. Photochromism into nanosystems: towards lighting up the future nanoworld, Chemical Society Reviews. 47 (2018) 1044-1097.

[20] V. Y. Reshetnyak, I. P. Pinkevych, D. R. Evans. Impact of photo-transformed molecules on two-beam energy exchange in hybrid photorefractive cholesteric cells, Journal of Molecular Liquids. 267 (2018) 45-55.

[21] H. Nemati, S. Y. Liu, A. Moheghi, et al. Enhanced reflection band broadening in polymer stabilized cholesteric liquid crystals with negative dielectric anisotropy, Journal of Molecular Liquids. 267 (2018) 120-126.

[22] P. J. Jessy, S. Radha, N. Patel. Morphological, optical and dielectric behavior of chiral nematic liquid crystal mixture: Study on effect of different amount of chrality, Journal of Molecular Liquids. 255 (2018) 215-223.

[23] L. A. Bulavin, L. N. Lisetski, S. S. Minenko, et al. Microstructure and optical properties of nematic and cholesteric liquid crystals doped with organo-modified platelets, Journal of Molecular Liquids. 267 (2018) 279-285.

[24] G. Barbero, W. C. Zheng, B. Zappone. Twist transitions and force generation in cholesteric liquid crystal films, Journal of Molecular Liquids. 267 (2018) 242-248.

[25] L. Wang, H. K. Bisoyi, Z. G. Zheng, et al. Stimuli-directed self-organized chiral superstructures for adaptive windows enabled by mesogen-functionalized graphene, Materials Today. 20 (2017) 230-237.

[26] L. Wang, H. Dong, Y. N. Li, et al. Reversible Near-Infrared Light Directed Reflection in a Self-Organized Helical Superstructure Loaded with Upconversion Nanoparticles, Journal of the American Chemical Society. 136 (2014) 4480-4483.

[27] L. Wang, W. L. He, X. Xiao, et al. Hysteresis-Free Blue Phase Liquid-Crystal-Stabilized by ZnS Nanoparticles, Small. 8 (2012) 2189-2193.

[28] L. Wang, A. M. Urbas, Q. Li. Nature-Inspired Emerging Chiral Liquid Crystal Nanostructures: From Molecular Self-Assembly to DNA Mesophase and Nanocolloids, Advanced Materials. 30 (2018) 1801335-1801376.

[29] J. W. Goodby. Chirality in Liquid Crystals, Journal of Materials Chemistry. 1 (1991) 307-318.

[30] G. H. Brown, J. J. Wolken. Liquid Crystals and Biological Structures, New York: Academic Press, 1979.

[31] I. Dierking. Textures of Liquid Crystals, Wiley-VCH, Weinheim, 2003.

[32] P. P. Crooker. The blue phases: A review of experiments, liquid Crystals. 5 (1988) 751-775.

[33] H. Stegemeyer, T. H. Blümel, K. Hiltrop, et al. Thermodynamic, structural and morphological studies on liquid-crystalline blue phases, liquid Crystals. 1 (1986) 3-28.

[34] J. Thoen. Adiabatic scanning calorimetric results for the blue phases of cholesteryl nonanoate, Physical Review A. 37 (1988) 1754-1759.

[35] J. S. Hu, D. Li, W. C. Zhang, et al. Synthesis, structure, and properties of chiral liquid crystal monomers and polymers based on menthol, Journal of Polymer Science Part a-Polymer Chemistry. 50 (2012) 5049-5059.

[36] J. S. Hu, X. F. Liu, Q. B. Meng, et al. New chiral liquid crystalline monomers, polymers, and elastomers derived from menthol derivatives: synthesis and mesomorphism, Journal of Materials Science. 49 (2014) 1229-1239.

[37] J. S. Hu, K. Q. Wei, B. Y. Zhang, et al. Synthesis, structure and properties of new chiral liquid crystalline monomers and homopolysiloxanes containing menthyl groups, Liquid Crystals. 35 (2008) 925-935.

[38] J. S. Hu, X. Zhang, Y. G. Jia, et al. Synthesis and phase behaviour of chiral liquid crystalline monomers based on menthyl groups, smectic polymers and cholesteric elastomers, Liquid Crystals. 39 (2012) 121-131.

[39] Y. G. Jia, J. S. Hu, D. Li, et al. Synthesis and phase behavior of chiral liquid crystalline polymeric networks derived from menthol, High Performance Polymers. 24 (2012) 673-682.

[40] C. C. Luo, Y. G. Jia, B. F. Sun, et al. The effect of chain length in terminal groups on the mesomorphic behavior of novel (-)-menthol-based chiral liquid crystal compounds with a blue phase, New Journal of Chemistry. 41 (2017) 3677-3686.

[41] Y. G. Jia, C. C. Luo, Z. X. Zhu, et al. Synthesis and properties of new (-)-menthol-derived chiral liquid crystal compounds with alkyl or alkoxy terminal groups, Liquid Crystals. 44 (2017) 526-537.

[42] C. C. Luo, Y. G. Jia, K. M. Song, et al. The effect of terminal alkoxy chain on mesophase behaviour, optical property and structure of chiral liquid crystal compounds derived from (-)-menthol, Liquid Crystals. 44 (2017) 2366-2378.

[43] S. L. Wu, T. S. Chen. Synthesis and frustrated phases of chiral liquid crystals derived from (R)-3-alkoxy-2-methylpropionic acids, Liquid Crystals. 32 (2005) 63-68.

[44] T. N. Chan, Z. Lu, W. S. Yam, et al. Non-symmetric liquid crystal dimers containing an isoflavone moiety, Liquid Crystals. 39 (2012) 393-402.

[45] P. A. Henderson, J. M. Seddon, C. T. Imrie. Methylene- and ether-linked liquid crystal dimers II. Effects of mesogenic linking unit and terminal chain length, Liquid Crystals. 32 (2005) 1499-1513.

[46] H. C. Lee, Z. Lu, P. A. Henderson, et al. Cholesteryl-based liquid crystal dimers containing a sulfur-sulfur link in the flexible spacer, Liquid Crystals. 39 (2012) 259-268.

[47] M. M. Naoum, A. A. Fahmi, N. H. S. Ahmed, et al. The effect of lateral methyl substitution on the mesophase behaviour of aryl 4-alkoxyphenylazo benzoates, Liquid Crystals. 42 (2015) 1627-1637.

[48] C. T. Imrie, L. Taylor. The preparation and properties of low molar mass liquid crystals possessing lateral alkyl chains, Liquid Crystals. 6 (1989) 1-10.

[49] M. M. Naoum, A. A. Fahmi, N. H. S. Ahmed, et al. The effect of inversion of the ester group on the mesophase behaviour of some azo/ester compounds, Liquid Crystals. 42 (2015) 1298-1308.

[50] D. J. Broer, J. Lub, G. N. Mol. Wide-Band Reflective Polarizers from Cholesteric Polymer Networks with a Pitch Gradient, Nature. 378 (1995) 467-469.

[51] M. Mitov. Cholesteric Liquid Crystals with a Broad Light Reflection Band, Advanced Materials. 24 (2012) 6260-6276.

[52] T. H. Lin, C. W. Chen, Q. Li. Self-Organized 3D Photonic Superstructure: Blue Phase Liquid Crystal, Anisotropic Nanomaterials: NanoScience and Technology, 2015, pp. 337-376.

[53] I. Nishiyama, E. Chin, J. W. Goodby. Ferrielectric and Antiferroelectric Properties of a Fluoro substituted Biphenyl Ester, Journal of Materials Chemistry. 3 (1993) 161-168.

[54] H. W. Huang, T. I. Kaneko, K. Horie, et al. Fluorescence study on intermolecular complex formation between mesogenic terphenyldiimide moieties of a thermotropic liquid-crystalline polyimide, Polymer. 40 (1999) 3821-3828.

Graphical Abstract

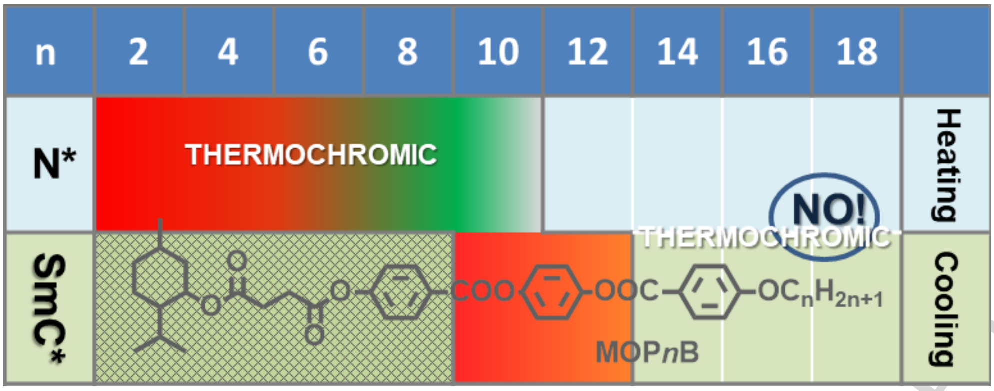

Highlights

Novel CLCs **MOP*n*B** based on (-)-menthol with high chirality were synthesized.

All chiral liquid crystals **MOP*n*B** displayed blue phase.

MOP*n*B (*n* = *2* - *10*) revealed the thermochromic property in N* phase on heating.

MOP*n*B (*n* = *10*, *12*) revealed the thermochromic property in SmC* phase on cooling.